Multi-Noise and Multi-Channel Derived Prior Information for Grayscale Image Restoration

MINGHUI ZHANG[1], YUAN YUAN[1], FENGQIN ZHANG[1], SIYUAN WANG[1],
SHANSHAN WANG [iD][2], **(Member, IEEE), AND QIEGEN LIU** [iD][1], **(Member, IEEE)**

[1]Department of Electronic Information Engineering, Nanchang University, Nanchang 330031, China
[2]Paul C. Lauterbur Research Center for Biomedical Imaging, Shenzhen Institute of Advanced Technology, Chinese Academy of Sciences, Shenzhen 518005, China

Corresponding authors: Shanshan Wang (sophiasswang@hotmail.com) and Qiegen Liu (liuqiegen@ncu.edu.cn)

ABSTRACT Image restoration is an extensively studied area with lots of outstanding algorithms developed. Nevertheless, most existing methods still have some limitations that only apply to a single tailored restoration task or suffer from long iterative reconstruction time or yield unstable results. To address these challenges, this work presents a multi-noise and multi-channel enhanced Deep Mean-Shift Prior (MEDMSP) for grayscale IR tasks. Specifically, we draw valuable high-dimensional prior knowledge by learning a multi-noise stimulated DMSP network from color images with RGB-channels. Variable augmentation technique is then adopted for incorporating the higher-dimensional network prior into the iterative reconstruction procedure. MEDMSP has been evaluated on different IR tasks and compared to a variety of state-of-the-art methods. Experimental results show that the proposed method has better capability in image deblurring and accurate compressive sensing reconstructions in terms of both visual and quantitative comparisons.

INDEX TERMS Image restoration (IR), multi-noise, multi-channel, deep mean-shift prior, iterative reconstruction.

I. INTRODUCTION

Image restoration (IR) is one of the most fundamental and popular topics in computational imaging. Its purpose is to recover the original high-quality image u from its degraded version y, whose typical degrading formulation can be described as follows:

$$y = Hu + n \qquad (1)$$

where H is a matrix representation of the degrading operator and n is additive white Gaussian noise. Various restoration scenarios are determined by different settings of H. For example, IR task could be deblurring for a blurring operator [1], denoising for an identity operation [2]–[4] and compressive sensing (CS) for an incoherently undersampling operator in frequency domain [5], [6].

Since IR is often ill-posed, prior knowledge is effectively adopted to recover the image, which can be obtained by

solving:

$$\min_u \|Hu - y\|^2 + \lambda\, prior(u) \qquad (2)$$

where $\|Hu - y\|^2$ is the l_2-norm data-fidelity term and $prior(u)$ denotes an image prior to resolve the regularization problem that weighted by parameter λ. To solve this problem, diverse model-based optimization methods have been developed, which normally have beautiful mathematical explanations and stable solutions [7]–[15]. Despite encouraging performances have been achieved, these methods tend to suffer from relatively time-consuming iterative procedures and still require improve recovery accuracy [16].

On the other hand, deep learning has shown great potential in computer vision [17], [18] and it becomes a popular choice to solve IR tasks [19]–[22]. These methods can be regarded as the discriminative learning approaches, which directly learn the parameters in prior term $prior(u)$ by optimizing a loss function on a number of clear-degraded image pairs. For instance, Burger et al. [19] firstly proposed to use the multi-layer perception (MLP) for image denoising.

Dong *et al.* [20] presented a straightforward 3-layer convolutional neural network (CNN) for super-resolution. It is worth noting that with increased capacity of network design and data collection, recent discriminative learning methods have achieved promising performances [23]–[26]. However, some discriminative learning methods only apply to a specialized IR task, which limits in flexibility and robustness. For example, even on the same specific task such as image deblurring [21], different models need to be trained separately for different blur kernels and noise circumstances.

Recognizing that each categories of methods has its own advantages and limitations, several researchers have attempted to incorporate discriminative learning into the model-based optimization to solve the general IR problems [27]–[30]. Especially, Zhang *et al.* [27] proposed a denoising convolutional neural network (DnCNN) for IR tasks with encouraging performances achieved. Unfortunately, a remaining drawback of DnCNN is its requirement for an expensive retraining whenever the scenarios (like the noise level, noise type or desired measure of fidelity) change a little bit. To address this issue, a denoising autoencoder priors (DAEP) was proposed for different IR tasks [29], [31]. Additionally, a deep mean-shift prior (DMSP) being proportional to the gradient of the logarithm of the image prior was also proposed in [30]. Both DAEP and DMSP train only one network and integrate it into the iterative restoration for different IR tasks. However, its output is unstable which tends to vary for different IR scenarios, but the performance can still be improved [16].

Based on the above observations, we urgently require a powerful neural network, which should not only be strongly applied to different IR tasks, but also has the advantages of stable model optimization. In this paper, we present a multi-noise and multi-channel enhanced prior dubbed as MEDMSP for grayscale IR tasks, which introduces two new key features for DMSP and a new iterative algorithm for incorporating high-dimensional prior into lower-dimensional task. Specifically, our contributions could be summarized as follows:

- Multi-noise stimulation is adopted for the prior design. To enable MEDMSP more robust and stable for different IR tasks, multi-noise weighted strategy is adopted. This design is motivated by the aggregation principle, indicating that the multi-noise stimulation can avoid getting into local solutions and make the iterative process more stable [16].
- Multi-channel information is used for training a high-dimensional prior, the merit of which is its capability in getting more valuable prior knowledge. This high-dimensional prior in MEDMSP is learned among R, G, B channels from color training images.
- An iterative algorithm has been introduced to incorporate the high-dimensional enhanced prior into grayscale IR task. MEDMSP can tackle non-convex minimization by adopting the proximal gradient and alternative iteration optimization. The proposed method has been tested

for different IR tasks, and outstanding performances have been achieved.

II. PRELIMINARY

IR is an ill-posed problem that should be regularized by effective priors to obtain acceptable solutions. Many classical models have been developed for the regularization-based image inverse problems, such as Tikhonov regularization [7] and the well-known total variation [8], [9]. Although this kind of methods effectively exploited the image local structure to preserve image edges and could characterize the piecewise constant signals well, they tended to over-smooth the image resulting in some image details loss. The sparsity-based techniques are more effective in representing local image structures. It assumed that the image patch can be precisely described with a few elemental structures from an off-the-shelf transformation matrix or a learned dictionary. Indeed, the IR community has witnessed a flurry of sparsity-based IR methods in the past decade [5], [10]–[15]. For example, Dong *et al.* proposed a hybrid method based on wavelet-transform and sparse-redundant representations model for IR [12]. Gu *et al.* put forward a weighted nuclear norm minimization (WNNM) with application to image denoising [15]. Dong *et al.* introduced a nonlocal low-rank regularization (NLR) approach toward exploiting both the group sparsity of similar patches and the non-convexity of rank minimization [5]. Lately, neural networks are attractive to solve IR since they allow for straightforward end-to-end learning [27]–[31]. In this paper we also try to explore neural networks as priors for grayscale IR tasks.

III. PROPOSED MEDMSP METHOD

Based on the naive DMSP model, this paper proposes a new prior MEDMSP by introducing two key new features and one new algorithm. First, multi-noise stimulation strategy is proposed to improve the stability and robustness of the prior. Second, high-dimensional prior information is obtained by employing multi-channel learning for denoising autoencoder (DAE) [29], [30]. Finally, proximal gradient method and alternating iteration are adopted to address the grayscale IR problem with the help of high-dimensional enhanced prior.

A. MULTI-NOISE STIMULATION

In [30], an interesting image prior $prior(u)$ expresses the image likelihood as the logarithm of the Gaussian-smoothed true natural image distribution, i.e.,

$$prior(u) = log \int g_\sigma(\eta)p(u+\eta)d\eta \qquad (3)$$

where $g_\sigma(\eta)$ represents a local Gaussian kernel with standard variance σ. $p(u+\eta)$ is true natural image distribution.

A crucial factor of DMSP is that they use a denoising autoencoder (DAE) to learn the gradient of the prior in Eq. (3). Concretely, the DAE network and the input image are represented as $r_\sigma(u)$ and u, respectively, and then the DAE output $r_\sigma(u)$ is trained by using Gaussian noise and an

expected quadratic loss:

$$L_{DAE} = E_{\eta,u}[\|u - r_\sigma(u + \eta)\|^2] \quad (4)$$

According to [31], it revealed that the output $r_\sigma(u)$ of the optimal DAE is related to the true data density $p(u)$ as:

$$r_\sigma(u) = u - \frac{E_\eta[p(x - \eta)\eta]}{E_\eta[p(x - \eta)]}$$
$$= u - \frac{\int g_\sigma(\eta)p(u - \eta)\eta d\eta}{\int g_\sigma(\eta)p(u - \eta)d\eta} \quad (5)$$

They use the Gaussian derivative definition to rewrite the numerator in Eq. (5) to remove η and obtain the relationship between the DAE and the desired gradient of prior.

$$r_\sigma(u) = u + \frac{\sigma^2 \nabla \int g_\sigma(\eta)p(u - \eta)\eta d\eta}{\int g_\sigma(\eta)p(u - \eta)d\eta}$$
$$= u + \sigma^2 \nabla \log \int g_\sigma(\eta)p(u - \eta)d\eta \quad (6)$$

Thus, the gradient of the prior can be written using the DAE error :

$$\nabla\, prior(u) = \nabla log \int g_\sigma(\eta)p(u + \eta)d\eta$$
$$= [(r_\sigma(u) - u)]\Big/\sigma^2 \quad (7)$$

where $r_\sigma(u)$ expresses the output of DAE. The DAE in Eq. (7) may be overfitted to noisy images [30]. To alleviate the deficiency, they reformulated the prior to perform stochastic gradient descent steps that include noise sampling [30] with:

$$prior(u) = log \int g_\sigma(\eta)p(u + \eta)d\eta$$
$$= log \int g_{\sigma_2}(\eta_2) \int g_{\sigma_1}(\eta_1)p(u + \eta_1 + \eta_2)d\eta_1 d\eta_2$$
$$\geq \int g_{\sigma_2}(\eta_2) \log[\int g_{\sigma_1}(\eta_1)p(u + \eta_1 + \eta_2)d\eta_1]d\eta_2$$
$$= prior_L(u) \quad (8)$$

where $\sigma_1^2 + \sigma_2^2 = \sigma^2$. Jensen's inequality is used in the third line of Eq. (8). This leads to a new lower bound for the prior, termed $prior_L(u)$. In ref. [30], the author addressed overfitting issue by using the new lower bound $prior_L(u)$ with $\sigma_1 = \sigma_2 = \sigma/\sqrt{2}$. Its gradient is:

$$\nabla prior_L(u)$$
$$= \frac{2}{\sigma^2} \int g_{\sigma/\sqrt{2}}(\eta_2)(r_{\sigma/\sqrt{2}}(u + \eta_2) - (u + \eta_2))d\eta_2 \quad (9)$$

They further approximated the integral with a single noise sample, which results in the stochastic evaluation of the gradient as:

$$\nabla\, prior_L^s(u) = 2(r_{\sigma/\sqrt{2}}(u + \eta_2) - u)\Big/\sigma^2 \quad (10)$$

From the aforementioned illustration, we are inspired to propose an enhanced DMSP prior for image restoration tasks.
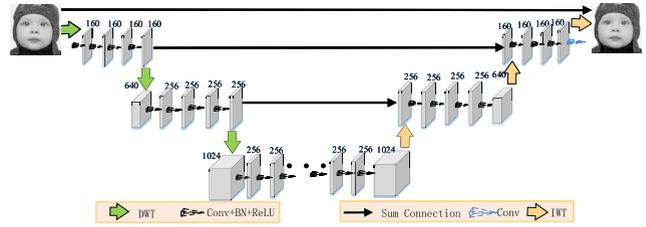

FIGURE 1. The MWCNN architecture with 3-level for single-channel grayscale image. Here DWT/IWT stands for the discrete/inverse wavelet transform.

FIGURE 2. A color image and its corresponding R, G, B components.

By introducing new components to explore more prior knowledge, we draw the prior of Eq. (10) with three noise implementations under different noise levels.

$$\nabla\, prior_L^s(u)$$
$$= \frac{1}{\sigma_1^2}(r_{\sigma_1/\sqrt{2}}(u + \eta_1) - u)$$
$$+ \frac{1}{\sigma_2^2}(r_{\sigma_2/\sqrt{2}}(u + \eta_2) - u) + \frac{1}{\sigma_3^2}(r_{\sigma_3/\sqrt{2}}(u + \eta_3) - u) \quad (11)$$

The multi-noise stimulation design is motivated by the aggregation principle, which shows multi-model implementation can avoid getting into local solutions and make the iterative process more stable [16]. Specifically, the extension involves two advantages: First, prior with three different noises leads to bigger model capacity, such as to enhance the representation ability. Second, three implementations also result in more robust. The rationality of setting the number of the multi-noise implementations in Eq. (11) to be three will be verified in the Experiment Section.

B. MULTI-CHANNEL ENHANCEMENT

Initially, we consider utilizing the multi-level wavelet-CNN (MWCNN) artchiecture [24] as a cornerstone to train $r_\sigma(u)$ for grayscale image restoration tasks. MWCNN is developed on the basis of multi-level wavelet packet transform (WPT) [30]. MWCNN extends WPT by adding a CNN block between any two levels of discrete wavelet transforms (DWTs). After each level of transform, all the subband images are taken as inputs to the CNN block, and then the compact representation is learned as an input to subsequent levels of DWT. As shown in Fig. 1, each CNN block is a 4-layer full connection without pooling and it takes all the subband images as input. Each layer of the CNN block is composed of convolution with 3×3 filters (Conv), batch normalization (BN), and rectified linear unit (ReLU) operations.
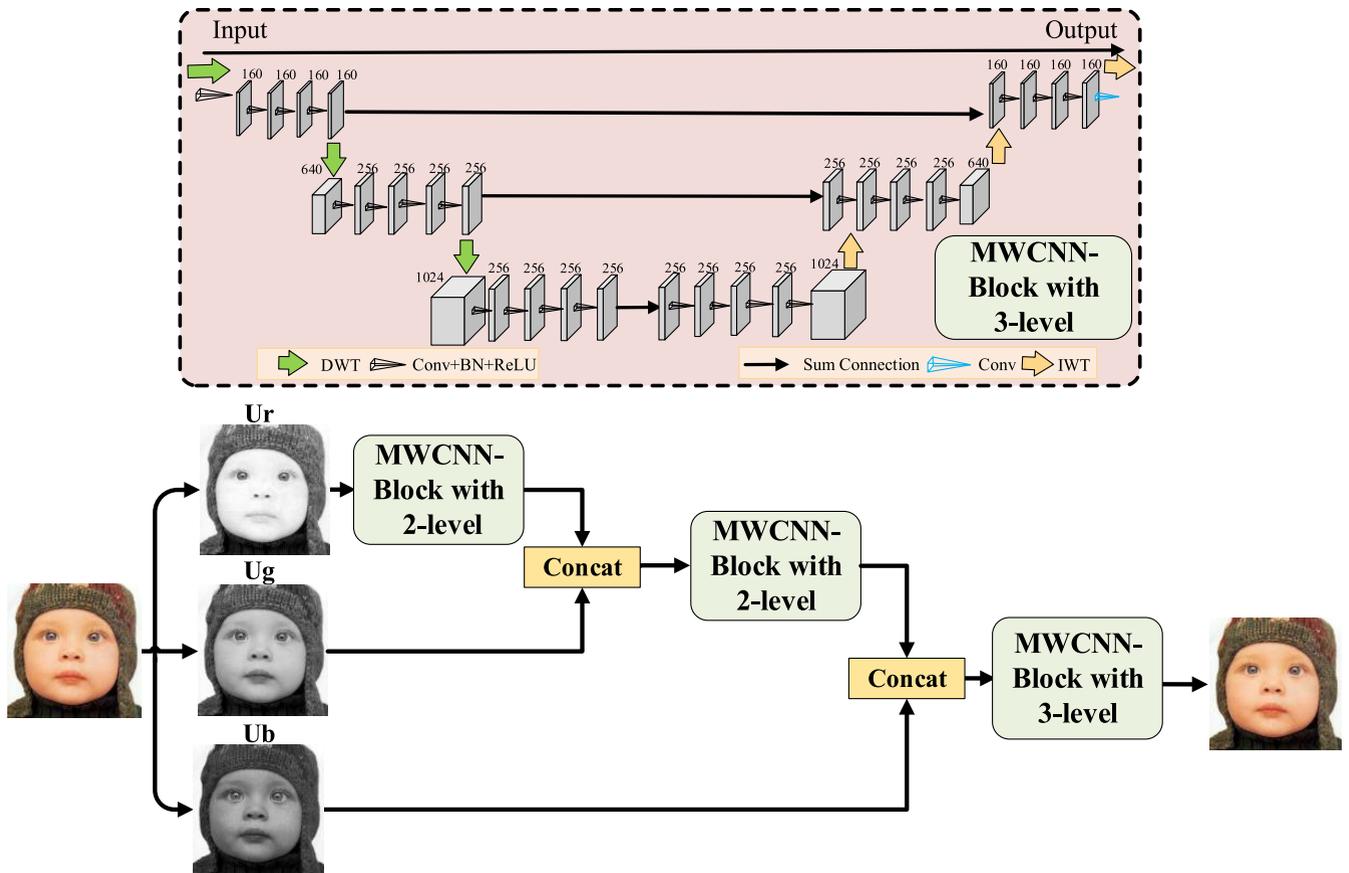
FIGURE 3. Visual example of the selected feature maps and the correlation analysis from MWCNN (a) and Dense-MWCNN (b).

As to the last layer of the last CNN block, Conv without BN and ReLU is adopted to predict residual image.

The second key component of the proposed MEDMSP is high-dimensional prior learning. The essence is to extend the representation dimension by training the network from color images with RGB-channels. Fig. 2 shows an illustration of a color image. We can see that the RGB channels are geometrical similar but exhibit different visual patterns. They possess more valuable prior knowledge compared to a single-channel grayscale image, which may provide the potential to better image quality.

At the network training phase, we assume channel number of the network input to be three and denote the vector variable $U = [U_1, U_2, U_3] = [U_r, U_g, U_b]$. Motivated by the spirit of densely connected convolutional network (DenseNet) [32], we employ the MWCNNs as blocks and densely connect them among RGB channels to form a higher-dimensional network DAE $r_\sigma(U)$, called Dense-MWCNN. As shown in Fig. 3, we employ a color image with artificial noise as input. As the levels of the DWT increases, the amount of calculation will increase accordingly. Considering the computational complexity and reconstruction effects, we chose to use a combination of two-level DWT and three-level DWT. First, we put the red component into the MWCNN-Block

with 2-level, and concatenate it with the green component to form a two-channel image. Then, we put the two-channel image into the MWCNN-Block with 2-level, and concatenate it with the blue component to generate a three-channel intermediate image. Finally, we put the three-channel image into the MWCNN-Block with 3-level to attain the estimation of image. It should be noted that the MWCNN-Block with 2-level only uses twice DWTs and IWTs but the MWCNN-Block with 3-level uses three times DWTs and IWTs.

To illustrate the advantages of the multi-channel learning strategy, we provide some denoising results for the high frequency subband and low frequency subband from the Dense-MWCNN in Fig. 4. At the same time, we show the feature maps and their correlations learned by MWCNN and Dense-MWCNN in Fig. 5. Specifically, the training set used by MWCNN is grayscale image, and the training set used by Dense-MWCNN is color image. The feature maps of the first convolution and its correlation after the third DWT in the third module of Dense-MWCNN and MWCNN. We choose 16 feature maps out of 256 by firstly clustering them into 16 groups, and then randomly select one feature map from each group to show as representative feature maps in Fig. 5. It can be observed that the feature map in Dense-MWCNN
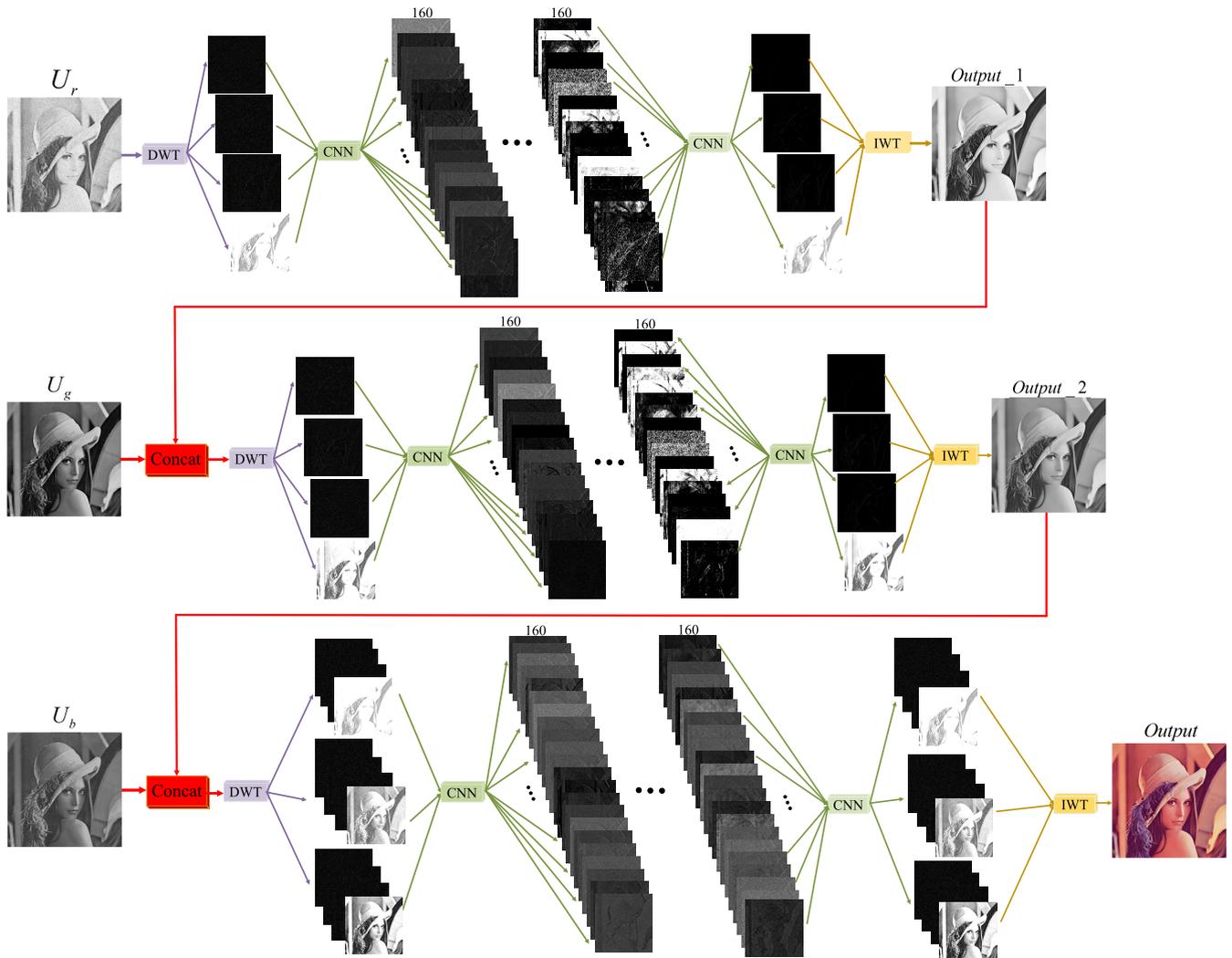
FIGURE 4. Visual example of denoising results for high frequency subband and low frequency subband in the Dense-MWCNN.

contains more information and detail features than that in MWCNN, indicating that the proposed network structure helps to obtain better feature representations. Additionally, we calculate the correlation among the 16 feature maps and visualize the similarity measure as a matrix. We can see that the correlation among feature maps in Dense-MWCNN is lower (blue corresponds to low correlation whereas red corresponds to high correlation). The lower the similarity between the feature maps, the more patterns between different feature maps. Hence, Dense-MWCNN in MEDMSP has a more diverse feature representation.

C. MEDMSP FOR IR

The last key feature of MEDMSP is how to explore the learned prior for IR tasks. As stated in Section III. A, it is desirable to exploit different levels of artificial noise, e.g. with standard variation σ_1, σ_2 and σ_3. If the standard variation σ_1 is set relatively small, there will be more texture details

in the restored image while introducing a large amount of noise. The σ_3 value is relatively large, and it prefers to produce smoother results but missing texture details. When the σ_2 value is set to be relatively medium, it contributes to the average result. Therefore, we can average them with the aim of preserving more details while removing more degradations.

After the multi-channel samples are trained, we turn to the restoration stage of single-channel image as shown in Fig. 6. In the restoration stage, variable augmentation technique is employed. At first, we copy and rearrange the single-channel image u into the same image with multi-channel formulation $U = [u, u, u]$. Since $\{U = [u, u, u]\} \subset \{U|U = [U_1, U_2, U_3]\}$, it paves the way to apply the trained multi-channel prior to the tested single-channel data. After the multi-channel procedure, we average the three output variable generated by the network to form the single-channel variable. Mathematically, by calculating the gradient of the
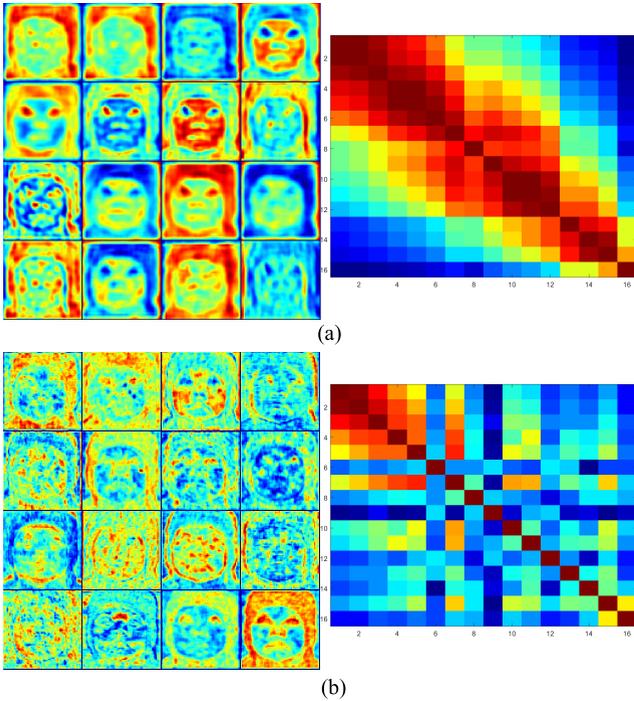
FIGURE 5. Visual example of the selected feature maps and the correlation analysis from MWCNN (a) and Dense-MWCNN (b).

high-dimensional prior, it yields:

$$
\begin{aligned}
&\nabla\, prior_L^s(U)\\
&= \frac{1}{\sigma_1^2}(r_{\sigma_1/\sqrt{2}}(U+\eta_1)-U)\\
&\quad + \frac{1}{\sigma_2^2}(r_{\sigma_2/\sqrt{2}}(U+\eta_2)-U) + \frac{1}{\sigma_3^2}(r_{\sigma_3/\sqrt{2}}(U+\eta_3)-U)
\end{aligned}
\tag{12}
$$

Then, the proposed MEDMSP model can be rewritten as a proximal gradient descent method:

$$
\begin{cases}
u^k = u^{k-1} - mean[\nabla\, prior_L^s(U^{k-1})]/\rho\\
u^{k+1} = \arg\min_u \|Hu-y\|^2 + \gamma\|u-u^k\|^2
\end{cases}
\tag{13}
$$

where ρ represents the gradient step size and γ denotes a balance parameter.

At each iteration, the intermediate results are obtained by employing the mean operator to the output of the three-channel network. As revealed at the previous section, this manipulation benefits from two aspects: One is that the image prior is guided from higher-dimensional structural prior. The other is that the multi-replication of the denoising operator facilitate better denoising and preserve more texture detail.

The second minimization in Eq. (13) is a standard least square (LS) problem, which can be solved as follows:

$$
(\gamma H^T H + 1)u^{k+1} = \gamma H^T y + u^k \tag{14}
$$

$$
u^{k+1} = \frac{\gamma H^T y + u^k}{(\gamma H^T H + 1)} \tag{15}
$$

Algorithm 1 MEDMSP

Enhanced Training Stage

For color training images $U = [U_r, U_g, U_b]$ collected from the dataset, crop it to be $192 \times 192 \times 3$ image blocks, and use the network in Fig. 3 to train the clear-noisy image pairs.

Robust Reconstruction Stage

  Initialization: $u^0 = H^T y$

  for $k = 1 \rightarrow K$ **do**

    1: Form the auxiliary variable $U^k = [u^k, u^k, u^k]$;

    2: Calculate $\nabla\, prior_L^s(U^k)$ in Eq. (12);

    3: $u^k = u^{k-1} - mean[\nabla\, prior_L^s(U^k)]/\rho$;

    4: Calculate $u^{k+1} = \frac{\gamma H^T y + u^k}{(\gamma H^T H + 1)}$ Eq. (15);

  end for

TABLE 1. Recovery PSNR/SSIMs of MEDMSP by varying the number of the multi-noise implementation for image Barbara with 15% random sampling pattern.

σ	PSNR/SSIM
$\sigma_1=3, \sigma_2=5, \sigma_3=8, \sigma_4=10$	29.88/0.8939
$\sigma_1=5, \sigma_2=8, \sigma_3=10$	29.80/0.8998
$\sigma_1=3, \sigma_2=5, \sigma_3=10$	29.69/0.8957
$\sigma_1=3, \sigma_2=8, \sigma_3=10$	29.77/0.8950
$\sigma_1=3, \sigma_2=10$	28.93/0.8825
$\sigma_1=5, \sigma_2=8$	28.61/0.8800
$\sigma_1=5, \sigma_2=10$	28.98/0.8833
$\sigma=3$	25.69/0.7937
$\sigma=5$	26.73/0.8363
$\sigma=8$	27.66/0.8491

IV. EXPERIMENTS

We implement the proposed architecture in Matlab and run all experiments on a desktop computer equipped with Intel Core i7-7700 central processing unit and GeForce Titan XP. Our training set is constructed by using images from DIV2K [33]. Concretely, we collect 400 images from DIV2K and cut the training images into $M = 91789$ patches with the size of 192×192 in the training stage. Image patches with different noisy levels are used to train models for learning a mapping from noisy images to de-noising results. Three models are used with the noise level $\sigma_1 = 3$, $\sigma_2 = 8$ and $\sigma_3 = 10$, respectively. The quality of the reconstruction is quantified by Peak Signal-to-Noise Ratio (PSNR) and Structural Similarity (SSIM) [34]. Testing images used in the experiments are depicted in Fig. 7.

A. ALGORITHM PROPERTY

In MEDMSP, employing the multi-noise implementation for the prior formulation and utilizing the multi-channel images as network input at training phase are two main innovations. In this section, we investigate the impact of these two features with different settings.

First, we investigate the optimal number for the multi-noise stimulation from 1 to 4. As can be observed in Table 1, when
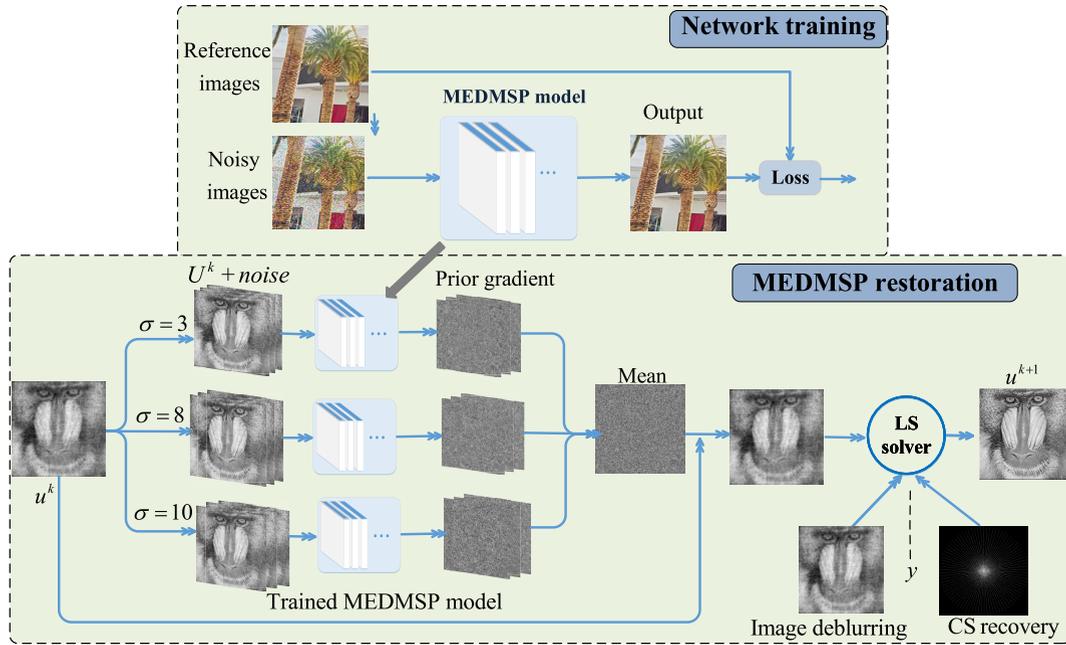
FIGURE 6. Illustration of the multi-channel network scheme at the training stage and the variable augmentation technique used for single-channel intermediate image at the iterative IR phase.

FIGURE 7. Six experimental test images: Barbara, Boats, Cameraman, Baboon, Pappers, Straw.
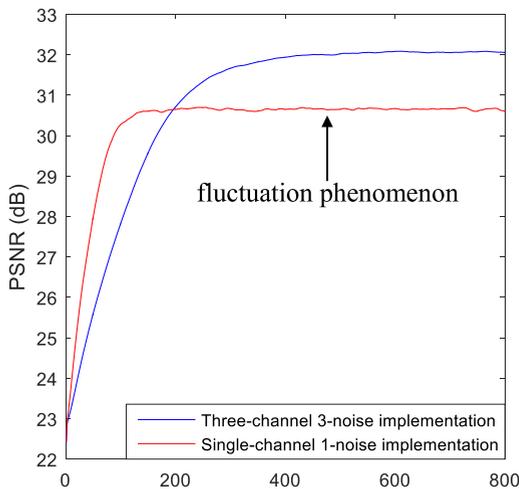

FIGURE 8. Convergence tendency of MEDMSP with three-channel 3-noise and single-channel 1-noise implementation.

the number of the multi-noise implementation increases, the obtained PSNR/SSIM values increase accordingly. The PSNR obtained with 2-noise implementation outperforms 1 dB than that with 1-noise implementation. 3-noise implementations gains 0.5 dB higher PSNR values than

that with 2-noise implementation. The PSNR obtained with 4-noise implementation is better than that with 3-noise implementation. However, as the number of the multi-noise stimulation increases, the computational cost becomes larger. Therefore, we set the number of multi-noise implementation to be 3.

Second, we study the impact of the multi-channel enhancement. Table 2 records the performance of MEDMSP with three-channel training data. It can be seen that, the PSNR values of three noises is higher than a single noise in terms of multi-channel and single-channel circumstances. Under three and single noise situation, the PSNR results using multi-channel are 0.67 dB and 0.68 dB higher than the single channel, respectively.

TABLE 2. Recovery PSNR/SSIMs of MEDMSP by varying the number of the multi-channel inputs for image Peppers with 15% random sampling pattern.

The channel number of input	PSNR/SSIM
$U = [U_1, U_2, U_3] = [U_r, U_g, U_b]$ $\sigma_1 = 3, \sigma_2 = 5, \sigma_3 = 10$	32.18/0.8839
$U = u, \sigma_1 = 3, \sigma_2 = 5, \sigma_3 = 10$	31.51/0.8781
$U = [U_1, U_2, U_3] = [U_r, U_g, U_b]$ $\sigma_1 = 8$	31.42/0.8764
$U = u, \sigma_1 = 8$	30.74/0.8659

Finally, the PSNR curve obtained utilizing three-channel 3-noise and single-channel 1- noise are shown in Fig. 8. We can see that both cases approximate to converge after around 200 iterations. Furthermore, MEDMSP not only

FIGURE 9. Visual quality comparison of image deblurring. Top: image Barbara on Gaussian kernel: 17 × 17, δ_d = 2.55. Middle: image Peppers on Gaussian kernel: 17 × 17, δ_d = 7.65. Bottom: image Boats on Gaussian kernel: 25 × 25, δ_d = 7.65. From left to right: noisy and blurred image, the deblurred images obtained by LevinSps, EPLL, DAEP, DMSP, DPE, MEDAEP and MEDMSP.

TABLE 3. Recovery PSNR/SSIMs of six test images under various blur size with different level noise.

Blur	Noisy		Barbara	Boats	Cameraman	Baboon	Peppers	Straw	Average
17	2.55	LevinSps	27.70/0.848	31.01/0.878	28.73/0.852	22.44/0.647	30.04/0.861	25.14/0.818	27.51/0.817
		EPLL	27.04/0.884	27.27/0.886	28.53/0.863	22.22/0.724	25.20/0.863	24.26/0.868	25.75/0.848
		DAEP	27.06/0.769	28.11/0.753	26.74/0.660	22.81/0.688	27.58/0.736	24.75/0.822	26.18/0.738
		DMSP	29.88/0.907	29.42/0.895	30.58/0.854	22.23/0.715	25.80/0.860	25.03/0.880	27.16/0.852
		DPE	29.84/0.882	31.08/0.873	30.18/0.839	22.87/0.763	29.86/0.843	26.38/0.901	28.37/0.849
		MEDAEP	30.94/0.903	32.42/0.902	**30.77/0.860**	23.11/0.724	31.50/0.871	**27.05/0.898**	29.30/0.860
		MEDMSP	**31.81/0.914**	**33.00/0.906**	30.65/0.833	**24.30/0.766**	**31.93/0.873**	26.87/0.897	**29.76/0.865**
	7.65	LevinSps	21.48/0.477	22.11/0.470	21.59/0.375	19.62/0.467	21.85/0.437	20.57/0.652	21.20/0.480
		EPLL	24.06/0.695	25.09/0.762	20.13/0.467	20.12/0.468	23.82/0.777	21.57/0.646	22.47/0.636
		DAEP	23.87/0.605	24.78/0.609	22.93/0.517	20.18/0.408	24.33/0.623	21.25/0.568	22.89/0.555
		DMSP	25.93/0.792	27.62/0.824	**27.85/0.798**	20.15/0.457	24.83/0.802	22.70/0.745	24.85/0.736
		DPE	24.96/0.637	26.05/0.631	25.59/0.547	20.40/0.510	25.65/0.607	22.91/0.734	24.26/0.597
		MEDAEP	24.85/0.723	27.65/0.801	26.70/0.800	20.14/0.442	27.45/0.804	22.24/0.625	24.84/0.700
		MEDMSP	**26.71/0.793**	**27.99/0.804**	27.36/0.806	**20.82/0.478**	27.62/0.806	**23.85/0.746**	**25.73/0.739**
25	2.55	LevinSps	28.33/0.854	30.92/0.886	28.65/0.850	21.72/0.604	29.52/0.857	24.87/0.824	27.34/0.811
		EPLL	26.05/0.842	26.64/0.872	27.90/0.849	21.09/0.645	23.97/0.829	23.20/0.822	24.80/0.810
		DAEP	26.93/0.779	27.63/0.768	26.48/0.665	21.58/0.625	26.38/0.731	24.38/0.828	25.56/0.733
		DMSP	27.10/0.878	26.22/0.869	28.83/0.826	21.24/0.642	23.07/0.815	23.60/0.836	25.01/0.811
		DPE	28.95/0.884	29.30/0.872	28.47/0.829	22.38/0.728	26.35/0.797	25.00/0.882	26.74/0.832
		MEDAEP	30.15/0.906	31.66/0.907	30.05/0.857	21.72/0.652	30.71/0.872	26.09/0.882	28.43/0.846
		MEDMSP	**31.62/0.904**	**33.49/0.920**	**30.16/0.801**	**23.47/0.733**	**31.02/0.864**	**26.80/0.878**	**29.43/0.850**
	7.65	LevinSps	21.24/0.393	21.58/0.373	21.53/0.260	19.39/0.412	21.45/0.339	19.98/0.589	20.86/0.395
		EPLL	23.46/0.670	25.04/0.771	25.28/0.780	19.81/0.441	23.16/0.765	21.50/0.652	23.04/0.680
		DAEP	23.90/0.608	24.84/0.629	23.35/0.516	19.91/0.439	23.95/0.608	21.79/0.640	22.96/0.573
		DMSP	25.05/0.777	25.02/0.798	26.64/0.779	19.95/0.480	22.69/0.760	21.87/0.727	23.51/0.720
		DPE	25.12/0.663	25.98/0.661	25.53/0.576	20.27/0.479	24.68/0.620	22.71/0.747	24.05/0.624
		MEDAEP	25.91/0.775	28.11/0.829	27.15/0.809	20.02/0.458	27.33/0.811	23.23/0.754	25.29/0.739
		MEDMSP	**27.91/0.819**	**29.38/0.848**	**27.40/0.790**	**21.03/0.504**	**28.34/0.808**	**23.34/0.708**	**26.23/0.746**

achieves higher value but also obtains more stable performance with multi-channel and multi-noise implementations, where fluctuation phenomenon has been avoided.

B. IMAGE DEBLURRING
In this section, we evaluate our method on image deblurring tasks, where two blur kernels in different sizes (i.e. 17 × 17

and 25 × 25, created from Matlab function fspecial) are used. Six grayscale images are tested to verify the performance of MEDMSP with comparison to local/nonlocal sparsity-enforcing methods including Levin *et. al.* [35] and EPLL framework [36], three deep prior derived methods containing Deep Prior Ensemble (DPE) [37], DAEP [29] and MEDAEP [38], and the baseline DMSP [30]. The setting

TABLE 4. Reconstruction PSNR/SSIMs of six test images at various sampling trajectories and sampling percentages.

		Barbara	Boats	Cameraman	Baboon	Peppers	Straw	Average
2D Random 15%	PANO	25.61/0.765	28.64/0.831	30.65/0.871	20.38/0.525	28.94/0.830	19.94/0.562	25.69/0.731
	NLR-CS	**30.23/0.899**	30.00/0.863	30.66/0.865	19.78/0.466	29.95/0.847	19.65/0.498	26.71/0.740
	BM3DRec	29.93/0.876	32.22/0.898	32.16/0.908	21.11/0.510	31.82/0.873	20.87/0.544	28.01/0.768
	ADMM-Net	26.69/0.788	29.61/0.855	31.21/0.879	20.61/0.515	29.92/0.850	20.93/0.586	26.49/0.746
	DMSP-MWCNN	29.27/0.884	31.13/0.888	30.76/0.868	20.31/0.494	30.68/0.866	20.78/0.587	27.16/0.764
	DC-CNN	25.77/0.750	29.88/0.745	31.10/0.836	20.24/0.473	31.10/0.844	20.10/0.539	26.37/0.715
	MEDMSP	29.91/0.900	**32.58/0.912**	**32.99/0.901**	**21.02/0.603**	32.25/0.887	**21.30/0.681**	**28.34/0.814**
Pseudo Radial 10%	PANO	24.46/0.702	27.96/0.815	28.45/0.849	19.88/0.469	27.92/0.812	19.45/0.512	24.69/0.693
	NLR-CS	**27.31/0.813**	28.65/0.832	29.00/0.848	19.55/0.411	28.63/0.831	19.37/0.441	25.42/0.696
	BM3DRec	25.63/0.720	30.38/0.846	29.48/0.864	20.70/0.469	**30.83/0.857**	20.07/0.486	26.18/0.707
	ADMM-Net	25.32/0.707	28.86/0.821	29.36/0.853	19.80/0.467	28.83/0.815	19.87/0.521	25.34/0.697
	DMSP-MWCNN	26.13/0.801	29.42/0.856	29.83/0.864	19.80/0.523	29.37/0.850	19.81/0.572	25.73/0.744
	DC-CNN	24.51/0.682	28.49/0.819	27.57/0.782	19.54/0.453	28.79/0.829	19.01/0.432	24.65/0.666
	MEDMSP	27.23/0.832	**30.57/0.874**	**30.09/0.883**	20.24/0.541	30.82/0.869	**20.22/0.593**	**26.53/0.766**

of parameter λ in MEDMSP is the same as that in DMSP.

The PSNR and SSIM values of test images by various blur kernels with different level noise are summarized. As shown in Table 3, MEDMSP produces the best average PSNR/SSIM values among all comparative methods. Specifically with the blurring kernel size to be 25×25, the average PSNR value of MEDMSP gains over nearly 3dB than that in the naive DMSP. Thus, we can deduce that the proposed MEDMSP method yields highly competitive performance compared with other leading deblurring methods at various noise variances and blur kernel sizes.

Visual quality comparisons of image deblurring at blurring kernel size 9×9 and Gaussian noise level $\delta_d = 7.65$ for image Peppers, blur kernel size 9×9 and Gaussian noise level $\delta_d = 2.55$ for image Barbara and blurring kernel size 17×17 and Gaussian noise level $\delta_d = 2.55$ for gray image Boats are shown in Fig. 9. it can be observed that LevinSps and DPE can deblur better but retain a lot of noise, and DAEP can remove noise better while the image is still blurry. EPLL can well reconstruct the piecewise smooth regions but often fails to recover fine image details. MEDAEP can remove noise better, but the reconstructed is too smooth to recover fine detail of image. MEDMSP can not only remove noise but also preserve the structure details. More specifically, it produces cleaner and sharper image edges and textures than other competing methods.

C. CS RECOVERY

This session evaluates the proposed method for CS recovery. Comparison experiments are conducted to test images using a variety of sampling schemes, with different under-sampling factors and patterns. The proposed method MEDMSP is compared with the reference-derived sparse representation method PANO [6], grouped low-rank based method NLR-CS [5], reconstruction method based on decoupling BM3D (BM3DRec) [39], the end-to-end deep architecture ADMM-Net [40], DC-CNN [41] and the baseline DMSP-MWCNN. DMSP-MWCNN is a hybrid algorithm that employing MWCNN as the learnt network in DMSP scheme.

Table 4 exhibits the PSNR and SSIM results of these methods. It can be observed that MEDMSP achieves the best values for all sampling ratios and test images. The average PSNR values obtained by BM3DRec and DMSP-MWCNN rank in the second and third at all sampling rates, respectively. Supervised learning ADMM-Net is comparable to the sophisticated model-based approach NLR-CS, yet is inferior to the higher-dimensional modeling of BM3DRec and MEDMSP. Moreover, PANO and DC-CNN are not ideal when recovering natural images.
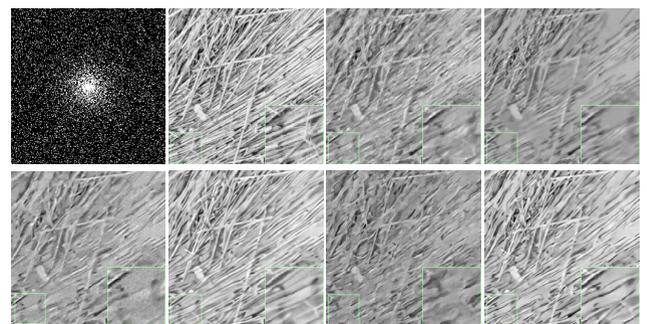
FIGURE 10. Recovery results at 15% random sampling. From left to right: Mask, Original, PANO, NLR-CS, BM3DRec, DMSP-MWCNN, DC-CNN and MEDMSP.

Figs. 10 and 11 show the visual comparisons on two test images. In Fig. 10, the reconstruction with MEDMSP method exhibits higher resolution than those with PANO and
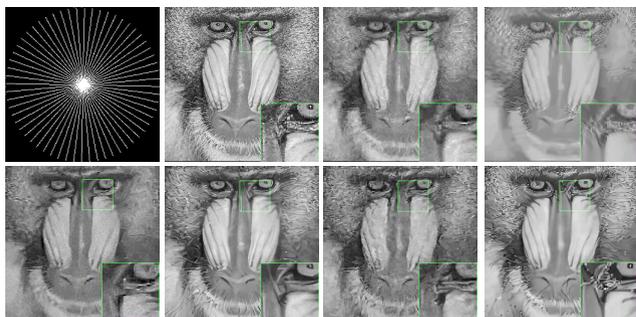
FIGURE 11. Recovery results at 10% radial sampling. From left to right: Mask, Original, PANO, NLR-CS, BM3DRec, DMSP-MWCNN, DC-CNN and MEDMSP.

NLR-CS, and there is almost devoid of aliasing artifacts. The single-channel based DMSP-MWCNN still exists some artifacts. The restored image of DC-CNN is more blurred. At the same time, the reconstruction depicted in Fig. 11 also indicates that MEDMSP preserves the texture details well. Moreover, we present an enlargement area to reveal the structures and fine details preserved by each algorithm. As can be observed in the zoom-in regions enclosed by green box, only the proposed MEDMSP successfully preserves the vertical line-like pattern.

V. CONCLUSION

This work proposes a MEDMSP for IR tasks with two new features introduced, namely, multi-noise stimulation and multi-channel enhancement. An iterative algorithm is also introduced, which paves a new way to explore the higher-dimensional network-induced prior information for low level IR tasks. The proposed method not only possesses the merits of the powerful neural network for drawing valuable prior knowledge but also has the stability of model-based methods. The robustness of the proposed method has been tested on different IR tasks such as image deblurring and compressive reconstruction, with superior performances achieved compared to state-of-the-art methods.

REFERENCES

[1] A. Beck and M. Teboulle, "Fast gradient-based algorithms for constrained total variation image denoising and deblurring problems," *IEEE Trans. Image Process.*, vol. 18, no. 11, pp. 2419–2434, Nov. 2009.

[2] K. Dabov, A. Foi, V. Katkovnik, and K. Egiazarian, "Image denoising by sparse 3-D transform-domain collaborative filtering," *IEEE Trans. Image Process.*, vol. 16, no. 8, pp. 2080–2095, Aug. 2007.

[3] Y. Chen and K. J. R. Liu, "Image denoising games," *IEEE Trans. Circuits Syst. Video Technol.*, vol. 23, no. 10, pp. 1704–1716, Oct. 2013.

[4] J. Dai, O. C. Au, L. Fang, C. Pang, F. Zou, and J. Li, "Multichannel nonlocal means fusion for color image denoising," *IEEE Trans. Circuits Syst. Video Technol.*, vol. 23, no. 11, pp. 1873–1886, Nov. 2013.

[5] W. Dong, G. Shi, X. Li, Y. Ma, and F. Huang, "Compressive sensing via nonlocal low-rank regularization," *IEEE Trans. Image Process.*, vol. 23, no. 8, pp. 3618–3632, Aug. 2014.

[6] X. Qu, D. Guo, B. Ning, Y. Hou, Y. Lin, S. Cai, and Z. Chen, "Undersampled MRI reconstruction with patch-based directional wavelets," *Magn. Reson. Imag.*, vol. 30, no. 7, pp. 964–977, Sep. 2012.

[7] H. W. Engl, K. Kunisch, and A. Neubauer, "Convergence rates for Tikhonov regularisation of non-linear ill-posed problems," *Inverse Problems*, vol. 5, no. 4, p. 523, 1989.

[8] L. I. Rudin, S. Osher, and E. Fatemi, "Nonlinear total variation based noise removal algorithms," *Phys. D, Nonlinear Phenomena*, vol. 60, nos. 1–4, pp. 259–268, 1992.

[9] A. Chambolle, "An algorithm for total variation minimization and applications," *J. Math. Imag. Vis.*, vol. 20, no. 1, pp. 89–97, 2004.

[10] M. Elad and M. Aharon, "Image denoising via sparse and redundant representations over learned dictionaries," *IEEE Trans. Image Process.*, vol. 15, no. 12, pp. 3736–3745, Dec. 2006.

[11] J. Yang, J. Wright, T. Huang, and Y. Ma, "Image super-resolution as sparse representation of raw image patches," in *Proc. IEEE Conf. Comput. Vis. Pattern Recognit.*, Jun. 2008, pp. 1–8.

[12] J. Mairal, M. Elad, and G. Sapiro, "Sparse representation for color image restoration," *IEEE Trans. Image Process.*, vol. 17, no. 1, pp. 53–69, Jan. 2008.

[13] W. Dong, X. Li, L. Zhang, and G. Shi, "Sparsity-based image denoising via dictionary learning and structural clustering," in *Proc. IEEE Conf. Comput. Vis. Pattern Recognit.*, Jun. 2011, pp. 457–464.

[14] W. Dong, L. Zhang, G. Shi, and X. Li, "Nonlocally centralized sparse representation for image restoration," *IEEE Trans. Image Process.*, vol. 22, no. 4, pp. 1620–1630, Apr. 2013.

[15] S. Gu, L. Zhang, W. Zuo, and X. Feng, "Weighted nuclear norm minimization with application to image denoising," in *Proc. IEEE Conf. Comput. Vis. Pattern Recognit.*, Jun. 2014, pp. 2862–2869.

[16] G. Alain and Y. Bengio, "What regularized auto-encoders learn from the data-generating distribution," *Comput. Sci.*, vol. 15, no. 1, pp. 3563–3593, 2012.

[17] A. Krizhevsky, I. Sutskever, and G. E. Hinton, "Imagenet classification with deep convolutional neural networks," in *Proc. Adv. Neural Inf. Process. Syst.*, 2012, pp. 1097–1105.

[18] K. Simonyan and A. Zisserman, "Very deep convolutional networks for large-scale image recognition," 2014, *arXiv:1409.1556*. [Online]. Available: https://arxiv.org/abs/1409.1556

[19] H. C. Burger, C. J. Schuler, and S. Harmeling, "Image denoising: Can plain neural networks compete with BM3D?" in *Proc. IEEE Conf. Comput. Vis. Pattern Recognit.*, Jun. 2012, pp. 2392–2399.

[20] C. Dong, C. C. Loy, K. He, and X. Tang, "Image super-resolution using deep convolutional networks," *IEEE Trans. Pattern Anal. Mach. Intell.*, vol. 38, no. 2, pp. 295–307, Feb. 2015.

[21] L. Xu, J. S. J. Ren, C. Liu, and J. Jia, "Deep convolutional neural network for image deconvolution," in *Proc. Adv. Neural Inf. Process. Syst.*, 2014, pp. 1790–1798.

[22] S. Wang, Z. Su, L. Ying, X. Peng, S. Zhu, F. Liang, D. Feng, and D. Liang, "Accelerating magnetic resonance imaging via deep learning," in *Proc. IEEE Int. Symp. Biomed. Imag.*, Apr. 2016, pp. 514–517.

[23] S. Liu, J. Pan, and M.-H. Yang, "Learning recursive filters for low-level vision via a hybrid neural network," in *Proc. Eur. Conf. Comput. Vis.*, 2016, pp. 560–576.

[24] P. Liu, H. Zhang, K. Zhang, L. Lin, and W. Zuo, "Multi-level wavelet-CNN for image restoration," in *Proc. IEEE Conf. Comput. Vis. Pattern Recognit. Workshops*, Jul. 2018, pp. 773–782.

[25] B. Lim, S. Son, H. Kim, S. Nah, and K. M. Lee, "Enhanced deep residual networks for single image super-resolution," in *Proc. IEEE Conf. Comput. Vis. Pattern Recognit. (CVPR) Workshops*, Jul. 2017, vol. 1, no. 2, p. 4.

[26] K. Zhang, W. Zuo, and L. Zhang, "Learning a single convolutional super-resolution network for multiple degradations," in *Proc. IEEE Conf. Comput. Vis. Pattern Recognit.*, vol. 6, Jun. 2018, pp. 3262–3271.

[27] K. Zhang, W. Zuo, Y. Chen, D. Meng, and L. Zhang, "Beyond a Gaussian Denoiser: Residual learning of deep CNN for image denoising," *IEEE Trans. Image Process.*, vol. 26, no. 7, pp. 3142–3155, Jul. 2017.

[28] K. Zhang, W. Zuo, S. Gu, and L. Zhang, "Learning deep CNN denoiser prior for image restoration," in *Proc. IEEE Conf. Comput. Vis. Pattern Recognit.*, vol. 2, Jul. 2017, pp. 3929–3938.

[29] S. A. Bigdeli and M. Zwicker, "Image restoration using autoencoding priors," 2017, *arXiv:1703.09964*. [Online]. Available: https://arxiv.org/abs/1703.09964

[30] S. A. Bigdeli, M. Zwicker, P. Favaro, and M. Jin, "Deep mean-shift priors for image restoration," in *Proc. Adv. Neural Inf. Process. Syst.*, 2017, pp. 763–772.

[31] P. Vincent, H. Larochelle, Y. Bengio, and P.-A. Manzagol, "Extracting and composing robust features with denoising autoencoders," in *Proc. 25th Int. Conf. Mach. Learn.*, 2008, pp. 1096–1103.

[32] G. Huang, Z. Liu, L. Van Der Maaten, and K. Q. Weinberger, "Densely connected convolutional networks," in *Proc. IEEE Conf. Comput. Vis. Pattern Recognit.*, Jul. 2017, pp. 4700–4708.

[33] E. Agustsson and R. Timofte, "NTIRE 2017 challenge on single image super-resolution: Dataset and study," in *Proc. IEEE Conf. Comput. Vis. Pattern Recognit. Workshops*, Jul. 2017, pp. 1122–1131.

[34] Z. Wang, A. C. Bovik, H. R. Sheikh, and E. P. Simoncelli, "Image quality assessment: From error visibility to structural similarity," *IEEE Trans. Image Process.*, vol. 13, no. 4, pp. 600–612, Apr. 2004.

[35] A. Levin, R. Fergus, F. Durand, and W. T. Freeman, "Image and depth from a conventional camera with a coded aperture," *ACM Trans. Graph.*, vol. 26, no. 3, p. 70, 2007.

[36] D. Zoran and Y. Weiss, "From learning models of natural image patches to whole image restoration," in *Proc. IEEE Int. Conf. Comput. Vis.*, Nov. 2011, pp. 479–486.

[37] R. Liu, L. Ma, Y. Wang, and L. Zhang, "Learning converged propagations with deep prior ensemble for image enhancement," *IEEE Trans. Image Process.*, vol. 28, no. 3, pp. 1528–1543, Mar. 2019.

[38] S. Li, B. Qin, J. Xiao, Q. Liu, Y. Wang, and D. Liang, "Multi-channel and multi-model-based autoencoding prior for grayscale image restoration," *IEEE Trans. Image Process.*, vol. 29, pp. 142–156, Jun. 2019.

[39] E. M. Eksioglu, "Decoupled algorithm for MRI reconstruction using nonlocal block matching model: BM3D-MRI," *J. Math. Imag. Vis.*, vol. 56, no. 3, pp. 430–440, Nov. 2016.

[40] Y. Yang, J. Sun, H. Li, and Z. Xu, "Deep ADMM-net for compressive sensing MRI," in *Proc. Adv. Neural Inf. Process. Syst.*, 2016, pp. 10–18.

[41] J. Schlemper, J. Caballero, J. V. Hajnal, A. Price, and D. Rueckert, "A deep cascade of convolutional neural networks for MR image reconstruction," in *Proc. Int. Conf. Inf. Process. Med. Imag.* Riverside, CA, USA: Springer, 2017, pp. 647–658.

MINGHUI ZHANG received the B.S. degree from Chongqing University, Chongqing, in 1990, majoring in biomedical engineering. He is currently with the Department of Electronic Information Engineering, Nanchang University, Jiangxi, China. His research interests include image compression and restoration, MRI reconstruction, and pattern recognition.

YUAN YUAN is currently pursuing the master's degree with the School of Information Engineering, Nanchang University. Her current research interests include wavelet sparse representations, deep learning, and image reconstruction.

FENGQIN ZHANG is currently pursuing the master's degree with the School of Information Engineering, Nanchang University. Her current research interests include CT reconstruction, wavelet transforms, multichannel learning, image restoration, and deep learning.

SIYUAN WANG is currently pursuing the master's degree with the School of Information Engineering, Nanchang University. His current research interests include wavelet transforms, multichannel learning, compressed sensing, deep learning, image processing, computer vision, and MRI.

SHANSHAN WANG received the B.S. degree in biomedical engineering from Central South University, Hunan, China, in 2009. She is currently pursuing the Ph.D. degree in biomedical engineering and computer science as a cotutelle student with Shanghai Jiao Tong University, Shanghai, China, and The University of Sydney, Sydney, NSW, Australia. She is working with the Paul C. Lauterbur Research Center for Biomedical Imaging, Shenzhen Institute of Advanced Technology. Her current research interests include inverse problem in medical imaging and image processing, such as MR/PET image reconstruction, image denoising, and dictionary learning.

QIEGEN LIU received the B.S. degree in applied mathematics from the Gannan Normal College, and the M.Sc. degree in computation mathematics and the Ph.D. degree in biomedical engineering from Shanghai Jiaotong University. Since 2012, he has been with the School of Information Engineering, Nanchang University, Nanchang, China, where he is currently an Associate Professor. He also holds a postdoctoral position at UIUC and the University of Calgary. His current research interests include compressed sensing, image reconstruction, and pattern recognition.

• • •